

Histopathological evaluation of prostate specimens after thermal ablation may be confounded by the presence of thermally-fixed cells

Mikael Anttinen, Eemil Yli-Pietilä, Visa Suomi, Pietari Mäkelä, Teija Sainio, Jani Saunavaara, Lauri Eklund, Roberto Blanco Sequeiros, Pekka Taimen & Peter J. Boström

To cite this article: Mikael Anttinen, Eemil Yli-Pietilä, Visa Suomi, Pietari Mäkelä, Teija Sainio, Jani Saunavaara, Lauri Eklund, Roberto Blanco Sequeiros, Pekka Taimen & Peter J. Boström (2019) Histopathological evaluation of prostate specimens after thermal ablation may be confounded by the presence of thermally-fixed cells, International Journal of Hyperthermia, 36:1, 915-925, DOI: [10.1080/02656736.2019.1652773](https://doi.org/10.1080/02656736.2019.1652773)

To link to this article: <https://doi.org/10.1080/02656736.2019.1652773>



© 2019 The Author(s). Published with license by Taylor & Francis Group, LLC



[View supplementary material](#)



Published online: 29 Aug 2019.



[Submit your article to this journal](#)



Article views: 314



[View related articles](#)



[View Crossmark data](#)

Histopathological evaluation of prostate specimens after thermal ablation may be confounded by the presence of thermally-fixed cells

Mikael Anttinen^a , Emil Yli-Pietilä^b, Visa Suomi^{c,d} , Pietari Mäkelä^c, Teija Sainio^c, Jani Saunavaara^c, Lauri Eklund^{e,f}, Roberto Blanco Sequeiros^d, Pekka Taimen^{e,f,*} and Peter J. Boström^{a,*}

^aDepartment of Urology, Turku University Hospital, Turku, Finland; ^bFaculty of Medicine, University of Turku, Turku, Finland; ^cDepartment of Diagnostic Radiology, University of Turku, Turku, Finland; ^dMedical Imaging Centre of Southwest Finland, Turku University Hospital, Turku, Finland; ^eInstitute of Biomedicine, University of Turku, Turku, Finland; ^fDepartment of Pathology, Turku University Hospital, Turku, Finland

ABSTRACT

Purpose: Prostate cancer can be eradicated with heat exposure. However, high and rapid temperature elevations may cause thermofixation giving the appearance of viable tissue. The purpose was to characterize the immunoprofile and evaluate the viability of prostate regions with suspected thermofixation.

Methods and materials: A prospective, ethics-approved and registered study (NCT03350529) enrolled six patients with MRI-visible, biopsy-concordant prostate cancer to undergo lesion-targeted MRI-guided transurethral ultrasound ablation (TULSA) followed by radical prostatectomy at 3 weeks, to evaluate the accuracy and efficacy of TULSA with whole-mount histology as a reference standard. If ambiguity about complete necrosis within the ablated region remained after hematoxylin-eosin staining, viability was assessed by immunohistochemistry. Treatment day MRI-thermometry and 3-week contrast-enhanced MRI post-TULSA were examined to assess ablation success and correlation with histopathology.

Results: One patient presented with an apparently viable subregion inside the ablated area, surrounded by necrosis on H&E staining, located where temperature was highest on MRI-thermometry and tissues completely devascularized on MRI. Immunoprofile of the apparently viable tissue revealed changes in staining patterns suggesting thermofixation; the most significant evidence was the negative cytokeratin 8 staining detected with Cam5.2 antibody. A comprehensive literature review supports these observations of thermofixation with similar findings in prostate and other tissues.

Conclusion: Thermally-fixed cells can sustain morphology on H&E staining. Misinterpretation of treatment failure may occur, if this phenomenon is not recognized and immunohistochemistry performed. Based on the previous literature and the current study, Cam5.2 staining for cytokeratin 8 appears to be a practical and reliable tool for distinguishing thermally-fixed from viable cells.

ARTICLE HISTORY

Received 31 May 2019
Revised 17 July 2019
Accepted 1 August 2019

KEYWORDS

Focal therapy; clinical trials-thermal ablation; noninvasive thermometry; physiological effects of hyperthermia; ultrasound



Introduction

Standard therapies for clinically significant localized prostate cancer (PCa) including radical prostatectomy (RP) and radiation therapy (RT) provide proven cancer control with improved survival [1–3], but carry the risk of treatment-related adverse effects to genitourinary and bowel function [4,5]. For selected patients, minimally invasive focal ablative therapies (FT) may offer an effective and less morbid alternative for PCa management. While FTs are increasingly utilized in the PCa management, they are considered experimental due to insufficient evidence confirming their longer-term oncological efficacy [6].


Most FTs in clinical practice use thermal energy to ablate prostate tissue, typically heating prostate tissue with radiofrequency, microwave, laser or high-intensity focused

ultrasound (HIFU) energy [7]. Some modern heat-based treatment systems exploit magnetic resonance imaging (MRI) for detecting and visualizing PCa lesions and guiding therapy into targeted regions [8–10].

MRI-guided transurethral ultrasound ablation (TULSA) is a novel therapy method for treating organ-confined PCa which has obtained promising results in terms of feasibility, safety and early efficacy [11–13]. TULSA delivers directional ultrasound from within the prostatic urethra to ablate prostate tissue [14]. By rapidly raising and maintaining elevated tissue temperatures above 55 °C, target tissue is destroyed primarily by undergoing acute coagulation necrosis and secondarily due to delayed thermal injury [15–18]. TULSA employs MRI-thermometry allowing real-time temperature changes to be monitored and subsequently used to control therapy so that

CONTACT Mikael Anttinen  mhjant@utu.fi  Department of Urology, Turku University Hospital, Kiinanmyllykatu 4-8, Turku, 20521 Finland

*These authors have contributed equally in this manuscript.

 Supplemental data for this article can be accessed [here](#).

© 2019 The Author(s). Published with license by Taylor & Francis Group, LLC

This is an Open Access article distributed under the terms of the Creative Commons Attribution License (<http://creativecommons.org/licenses/by/4.0/>), which permits unrestricted use, distribution, and reproduction in any medium, provided the original work is properly cited.

precise conformal ablative volumes can be achieved [19–22]. The ablated volume is visualized post-treatment on contrast-enhanced MRI as a non-perfused volume (NPV) indicating complete irreversible cell death [23–26]. The histopathological analyses of immediate and 3-week post-TULSA RP specimens have revealed accurate and precise ablation pattern with sharp demarcation of thermal injury. These treatment features of TULSA enable controlled ablation of prostate tumors with potentially reduced risk of damaging surrounding vulnerable tissues including the neurovascular bundles (NVB), bladder neck, pelvic floor muscles and rectal wall [11–13].

Although FTs appear promising for safe and efficient management of PCa, they continue to face challenges in determining how to monitor treatment efficacy and follow-up oncological outcome. Currently, the recommended follow-up measures after FT include prostate-specific antigen (PSA), prostate MRI and biopsy [6]. However, histopathological evaluation of prostate specimens after thermal ablation can be challenging due to various tissue changes related to heat-induced tissue destruction [16,17,27]. In general, three zones with a spectrum of specific morphological changes have been distinguished including a thermal fixation zone (TFZ), a coagulative necrosis zone (CNZ) and a margin zone (MZ) [17].

A high and rapid temperature rise in tissue may cause thermal fixation that retains tissue morphology in hematoxylin-eosin (H&E) staining suggesting untreated viable tissue [16,17,28–39]. Several studies have demonstrated the appearance of thermal fixation in various human tissues [32,37–39], including two treat-and-resect studies in RP specimens after thermal ablation with HIFU [16] and laser [36].

In clinical practice, thermally-fixed cells that appear viable on H&E after thermal ablation can confound histological assessment. If ancillary staining to identify thermofixation is not performed, this effect may lead to misdiagnosis of treatment failure and subsequently to incorrect treatment decisions.

Concept of thermal dose and mechanisms of cell death due to heat exposure

Therapeutic ultrasound generates heat by a thermoviscous effect where the mechanical energy of a propagating ultrasound wave is absorbed by tissue and converted into heat. The temperature rise caused by heating is dependent on the frequency and intensity of the ultrasound field as well as the physical properties of tissue including perfusion rate, thermal conduction and attenuation. These tissue properties are also temperature dependent, which further affects the heating efficacy. For instance, in prostate the perfusion rate has been shown to significantly increase during hyperthermia treatments [40], which reduces the temperature and consequently tissue thermal damage.

Thermal damage induced to tissue cells due to heating is not only dependent on temperature but also on the duration of heat exposure. To quantify the cumulative effect of both

temperature and time on cell injury, the metric of thermal dose was developed by Sapareto and Dewey [41]:

$$CEM_{43} = \int_0^{t_{\text{end}}} R^{43-T(t)} dt$$

where t_{end} is heating duration in minutes, T is temperature in °C and R is 0.25 for temperatures below 43 °C and 0.5 otherwise. The idea of thermal dose is to convert any time temperature combination of different thermal exposures to ‘cumulative equivalent-minutes’ at the temperature of 43 °C (CEM_{43}) which allows comparison using the same quantitative scale. By the definition of thermal dose, each one-degree increase in temperature above 43 °C halves the required heating duration for the same effective dose. The relationship between time and temperature for cell damage is therefore exponential, which has also been demonstrated in experimental studies [41,42]. For example, a heat exposure of one minute at 51 °C has the same thermal dose as 256 min at 43 °C (i.e., 256 CEM_{43}). Thus, thermal dose offers a simple but effective metric for determining treatment parameters for hyperthermia and thermal ablation therapies in clinical use.

The thermal dose scale does not require that different tissues have the same sensitivity to heat, and therefore, thresholds for cell damage and death due to heat exposure can be determined individually for each tissue type. Generally, a thermal dose of 240 CEM_{43} has been accepted as the threshold for cell death in thermal ablation modalities, such as HIFU therapy [43,44], where relatively rapid and high temperature elevations are used. However, some cell types are more resistant to heat than others, and therefore, the thermal dose required for cell damage or death should be tissue specific [42,45]. The differences in tissue thermal sensitivities are due to several reasons including the characteristics of protein structure, and the kinetics of repair and replacement processes [42]. For prostate tissue, it has been shown that thermal dose below 50 CEM_{43} causes no damage, 80 CEM_{43} causes minor damage and 240 CEM_{43} results in complete thermal coagulation [45].

It should be noted that there are a number of other factors which also affect the usage of thermal dose for measuring tissue damage. Tissues that have previously been exposed to heat might have acquired resistance to subsequent exposures at elevated temperatures (i.e., thermotolerance) [46], which in turn increases their thresholds for cell damage in terms of thermal dose. In addition, since the thermal dose metric was derived for the purpose of clinical hyperthermia treatments, there may be extrapolation inaccuracies when applying the metric to other thermal therapies where very low or very high temperatures are typical (i.e., outside the range of 39–57 °C) [42,47]. It is also assumed that the value of R is constant across a range of tissues with the breakpoint occurring at 43 °C, which might not always be the case [42,48]. Lastly, most of the data used to determine thermal dose thresholds in different tissues have been obtained from either animal or human cell line studies, which might not directly relate to the thermal sensitivity of human tissues *in vivo* [42,45].

The term 'thermal necrosis' generally refers to the stage of tissue after irreversible cell death due to heat exposure. However, necrosis only happens after cell death, and thus, the terms should not be used interchangeably [49]. Cell death due to thermal exposure can occur via multiple pathways. When relatively low temperatures below 60 °C are used, the primary mechanism of cell death is apoptosis where the internal cell structure is destroyed via a controlled process and without inflammation. In apoptotic cells, the nucleus of the cell is self-destroyed and its DNA is degraded by endonucleases [50]. At higher temperatures above approximately 60 °C, rapid protein denaturation occurs which leads to coagulative thermal necrosis (i.e., thermal ablation) [15]. At these 'high temperatures' collagen fibers gain enough energy to irreversibly transform from a uniform helical state to a more random state of lower organization [51,52].

Biology of thermal fixation

When the local temperature rise in tissue is sufficiently high and rapid, a process known as thermal fixation may also occur [32,35]. Thermally-fixed cells exhibit no visible morphological changes in traditional light microscopy, but closer investigation with scanning electron microscopy has shown them to lack nuclear membranes and organelle structures indicating irreversible cell death [37]. Thermal fixation appears to result from denaturation of the structural and enzymatic protein constituents of tissue, so that they are able to resist the typical repair/breakdown pathways of the body [32,34]. Therefore, thermally-fixed cells maintain their cytologic staining characteristics and preserved nuclear chromatin, which gives a histological staining appearance similar to viable cells [37]. This might lead to misinterpretation of histopathology results from thermal ablation therapies, when certain types of stains are used [16,37].

Objective

The purpose of this study was to characterize the immunoprofile and evaluate the viability of morphologically unaltered subregions of prostatic tissue within regions of coagulative necrosis on H&E staining after thermal ablation with TULSA. Multimodal analysis including treatment day MRI-thermometry, post-TULSA, 3-week NPV and comprehensive immunohistochemistry (IHC) were utilized for the assessment of the true nature and viability of the ablated tissue suspected to present thermal fixation. These results were contextualized by performing a comprehensive review of the applicable literature.

Material and methods

Study design

A prospective, registered (ClinicalTrials.gov Identifier: NCT03350529), single-center clinical phase-I study consented and enrolled six patients with MRI-visible, biopsy-concordant

localized PCa to undergo lesion-targeted TULSA (TULSA-PRO, Profound Medical Inc., Toronto, Canada; integrated into a 3T MR-system Ingenia 3.0T, Philips Healthcare, Best, Netherlands), followed by robot-assisted laparoscopic radical prostatectomy (RALP) at 3 weeks. The treat-and-3-week-resect setting enabled histological assessment of TULSA accuracy and efficacy including delayed thermal injury, but necessitated conservatively defined ablation zones to preserve surgical outcomes. In the vicinity of the neurovascular bundles (NVB), safety margins up to 3 mm were applied regardless of tumor extent, based on the concern that necrosis may migrate beyond the region of acute coagulation necrosis [18], potentially compromising the subsequent nerve-sparing RALP. All of the resected RALP specimens were formalin-fixed and paraffin-embedded for histopathological evaluation. The study protocol was approved by the local Ethics committee of the Hospital District of Southwest Finland, and written informed consent was obtained from all participants.

Initial histopathology of the whole-mount sections included H&E and IHC stainings. The evaluation was first performed under conventional light microscopy on glass slides and thereafter also on digital whole slide images. If complete and irreversible cell death of the ablated region remained ambiguous after H&E staining, comprehensive IHC was performed to characterize the immunoprofile and assess the viability of these regions. The staining pattern of the prostate glandular epithelium was assessed for CAM5.2 (cytokeratin 7 and 8), p16 and androgen receptor. AMACR (Alpha-methylacyl Coa racemase/P504S) was utilized to distinguish malignant glands from benign glands. Proliferation activity was assessed with Ki-67 staining, and thermal vascular damage was assessed with antibody to Factor VIII (von Willebrand Factor, vWF). All slides were examined by the same uropathologist with 10 years of experience in uropathology. The selected slides covering the ablation area were also examined by another uropathologist with more than 30 years of experience.

Data on treatment day MRI-thermometry and post-TULSA NPV at 3 weeks were also exploited to assess success of the ablation and the concordance of MRI findings with histopathology.

Histology and immunohistochemistry

The RALP specimens were fixed in 10% formalin and cut into approximately 5 mm sections with free hand as follows: apex and base in coronal plane, seminal vesicles in sagittal and mid-gland in transverse plane perpendicular to the long axis of the urethra. The entire material was embedded in paraffin using whole-mount macro-cassettes. Two 5- μ m sections from each block were cut for H&E staining and additional sections from selected blocks for IHC using BenchMark XT and ULTRA IHC/ISH automated slide staining instruments (Ventana Medical Systems, Tucson, Arizona, USA). All H&E slides were examined. The detailed list of utilized antibodies is shown in [Supplementary Table S1](#).

Histological image analysis

All H&E and IHC slides were scanned with NanoZoomer S60 (Hamamatsu Photonics, Hamamatsu, Japan) using the NDP.scan software (v. 3.2.12) and 20x scanning mode. Representative areas of each slide were captured with specific magnification pointing out region of interest in NDP.view2 software in which annotation was performed for all the slides. Two thermal damage boundaries were contoured: 1) the outer boundary of complete necrosis (complete and irreversible cell death) and 2) the outer limit of thermal injury (OLTI), outside which there was no visual evidence of thermal damage. The zone inside the complete necrosis boundary was defined as the coagulation necrosis zone (CNZ), and the zone between complete necrosis and the OLTI was defined as the margin zone (MZ).

Results

Study subjects

All of the six enrolled participants completed the study, and one of them presented with apparently viable tissue within the continuous area of coagulation necrosis on initial H&E staining (Figure 1). For this patient, comprehensive IHC was performed. The baseline clinical, MRI and tumor characteristics of this case are summarized in Figure 2(A) and described in detail below.

Treatment details and pathological evaluation with H&E staining

Patient 4 underwent lesion-targeted TULSA, with sonication and MRI times of 14 and 130 min, respectively. The MRI-thermometry derived maximum temperature and

thermal dose maps showed a homogeneous and continuous cytotoxic heating pattern extending into the prostate capsule and completely containing the targeted predefined region including the index tumor (Figure 2(B)). The 3-week NPV covered the targeted tumor without any enhancement observed inside the NPV indicating complete devascularization of the targeted region (Figure 2(C)). Further, the RALP procedure was uneventful without treatment-related complications.

H&E stained analysis of the RALP specimen from the same patient indicated a distinct round-shaped focus of morphologically viable adenocarcinoma in two consecutive slides 5 mm apart from each other, retaining nuclear and cytological details and resembling predominantly Gleason pattern 4 disease. The focus was situated within the ablated area, surrounded by CNZ (Figure 3). The surrounding CNZ was characterized by retention of cellular outline but loss of cytoplasmic and nuclear details, and the presence of hemorrhage and loosely woven collagen.

Interestingly, the region that appeared viable on H&E staining was located in the zone where the highest temperatures were reached based on MRI-thermometry data and was within a region of uniformly non-enhancing tissue on contrast-enhanced MRI. Quantitatively, the closest distance from the edge of the thermally-fixed region to the urothelium of the urethra was 8 mm, matching the 8 mm distance from the urothelium of the urethra to the maximum temperatures of 83.3 °C on MRI-thermometry. Furthermore, this patient differed from the other five study patients based on the finding that this patient had the fastest heat response of all treatments (time from start of heating to peak: 12 °C/min vs. median 7 °C/min (range: 5.2–10)) possibly explaining occurrence of thermal fixation in this case.

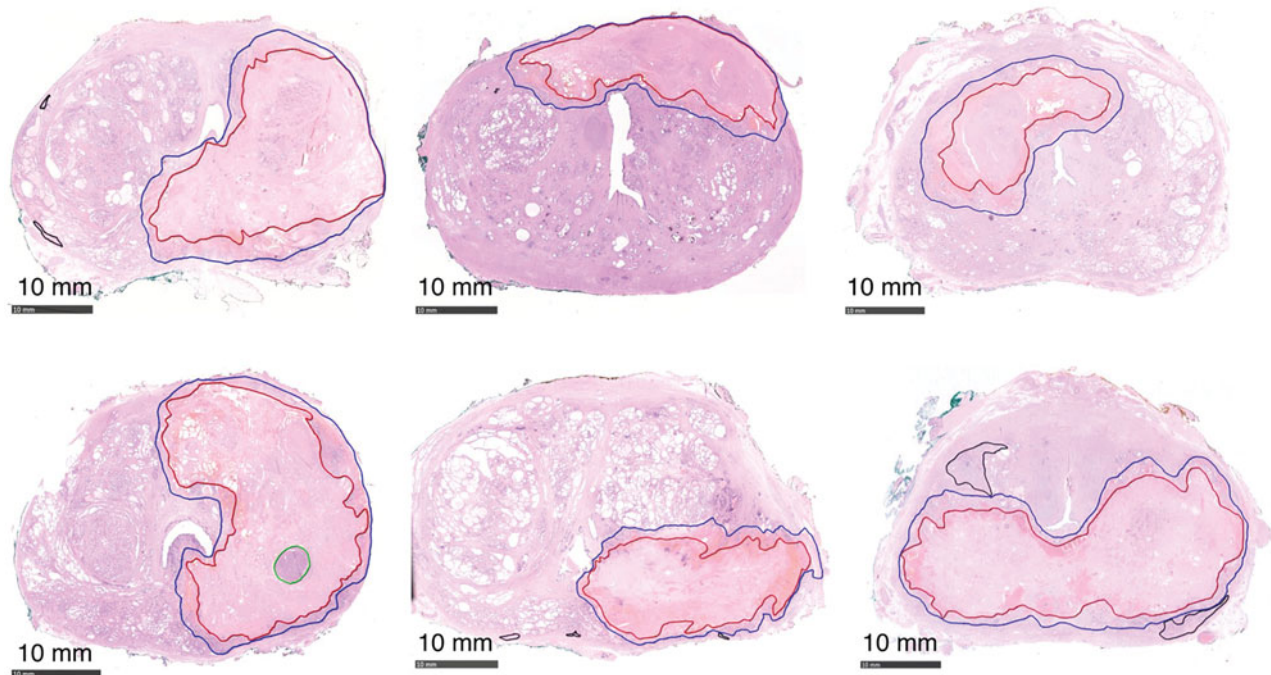


Figure 1. Annotated H&E stained axial whole-mount slide mid from the RALP specimen from every study patient. All patients except patient four presented complete coagulation necrosis of the targeted tumor: the complete irreversible cell death inside the red boundary (CNZ) and margin zone between red and blue boundaries (MZ). Patient 4 presented thermally-fixed viable-looking cells within green boundaries. Black contoured regions present outfield (outside treatment boundaries) residual prostate cancer.

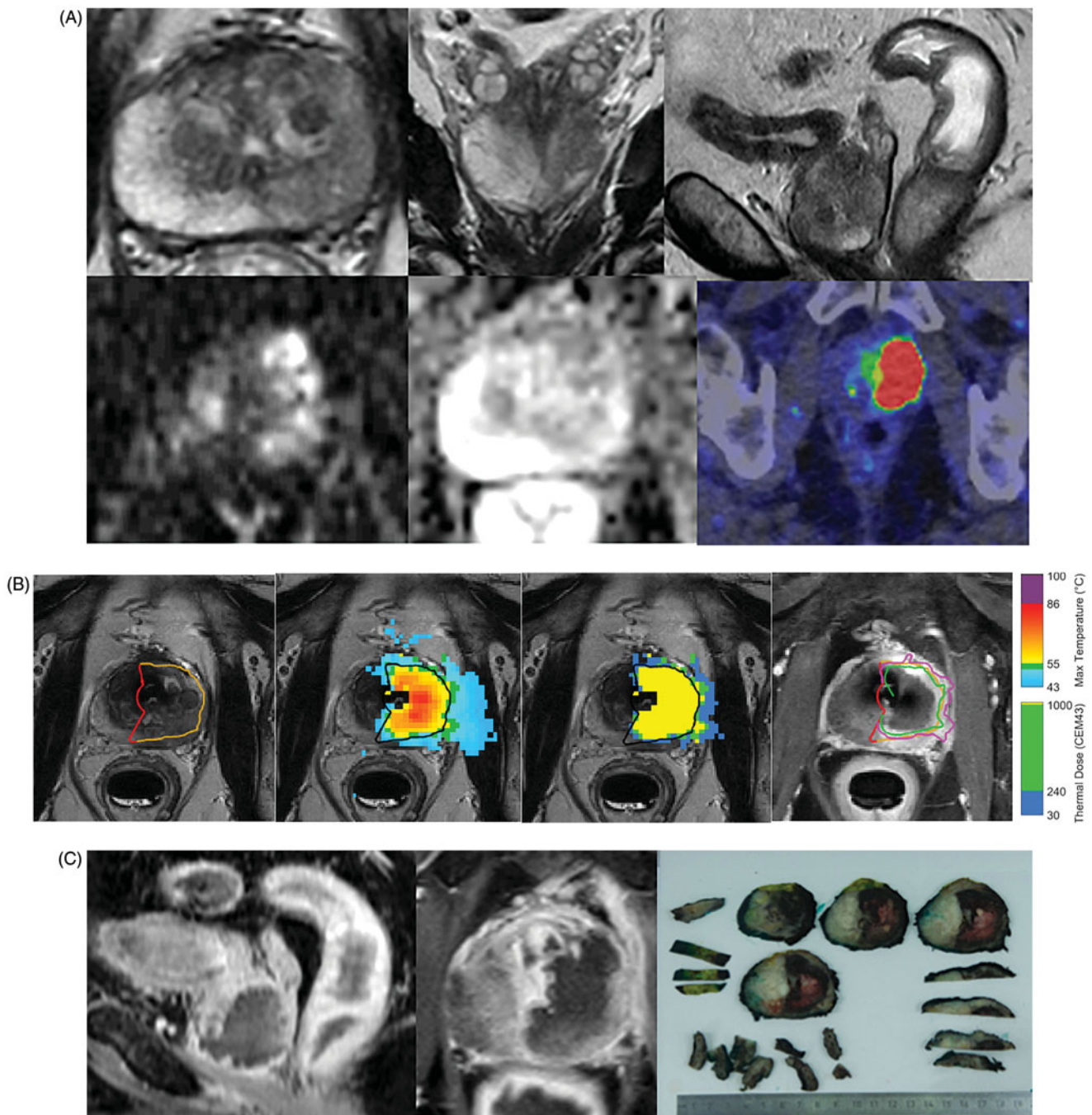


Figure 2. (A) Patient 4: A 70-year-old (ECOG 0, prostate volume 51 cc, BMI 30) Caucasian man without urinary symptoms and with elevated PSA level 36 ng/mL underwent pre-biopsy prostate MRI showing a left lobe situated 5.1 cc PIRADS 5 lesion in the close contact with prostate capsule. Axial, coronal and sagittal T2-weighted images on top panel (left to right in order); diffusion weighted and apparent diffusion coefficient images on bottom panel (left and middle) from the PIRADS 5 lesion. All the MRI-targeted 6-core biopsies confirmed Gleason Score $4+3=7$ PCa within the dominant lesion with cancer core length of 53 mm. The whole-body contrast-enhanced computer tomography (CT) and bone scintigraphy were both negative for metastasis. F18-prostate-specific membrane antigen (PSMA) positron emission tomography-CT excluded distant metastasis and showed an intensive PSMA-uptake with standardized uptake value maximum of 81.1 g/mL in the left lobe of the prostate concordant with the MRI (on bottom panel left). (B) Immediate post-treatment overlay images have been demonstrated from the active element of the patient 4: on the left targeted region; on the middle maximum temperature and thermal dose maps and on the right non-perfused volume (NPV). Yellow boundary demonstrates targeted region on treatment planning, purple 240 CEM43 isodose boundary and green 55° isotherm boundary. (C) This figure presents post-TULSA NPV on sagittal and axial images at 3 weeks just prior to RALP procedure and the sliced RALP specimen on the right, in which thermal damage region is clearly identified as the dark regions on the gross specimen.

Immunohistochemistry of areas suspected to present thermal fixation

IHC revealed that neither the apparently viable region nor the surrounding CNZ stained positively for cytokeratin 8, as assessed by Cam5.2 antibody (Figure 4). Conversely, both the

untreated benign region and apparent residual carcinoma just outside the ablated area were cytokeratin 8 positive (Figure 4). These observations suggest that negative cytokeratin 8 staining against a background of positive-staining untreated tissue can identify both thermally-fixed and thermally-necrosed cells.

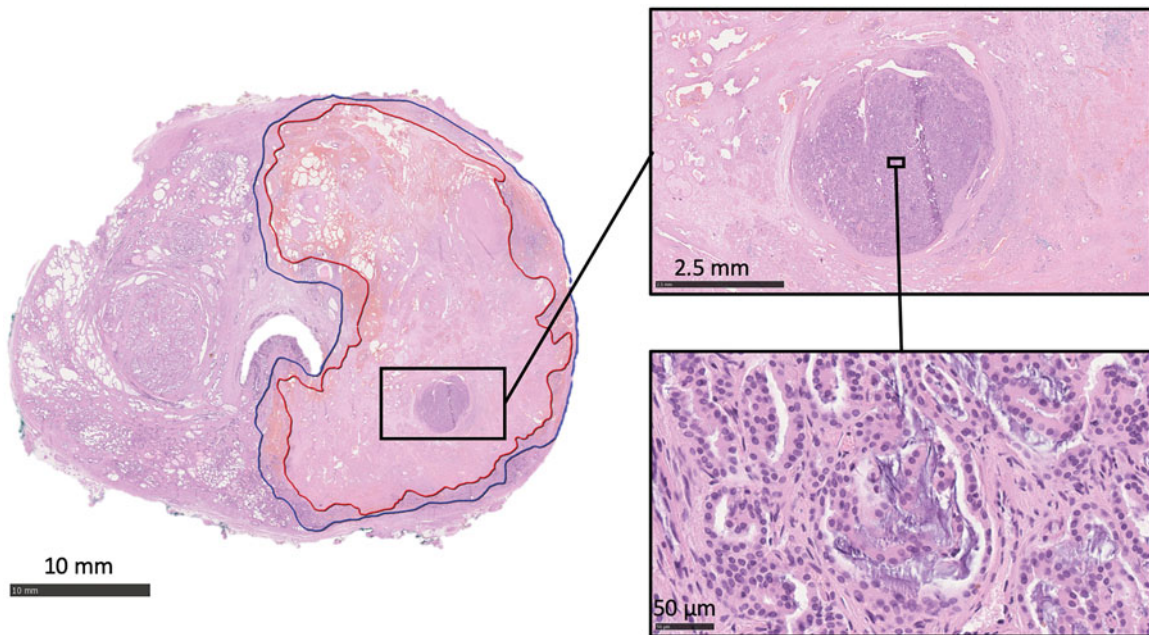


Figure 3. Histological analysis of prostatic thermal injury. An annotated axial H&E-stained whole-mount slide mid from the RALP specimen of the patient four showing the complete irreversible cell death inside the red boundary (CNZ) and margin zone between red and blue boundaries (MZ). Magnification H&E images from thermally-fixed area show well preserved morphology of Gleason 4 adenocarcinoma.

The patient presented abnormally excessive vWF immunostaining in the CNZ and MZ due to thermally injured blood vessels and leakage of plasma and platelets into the interstitial tissue. Both the apparently viable and untreated regions on H&E staining presented normal vWF immunostaining (Figure 4). These observations suggest a lack of vascular damage within thermally-fixed regions.

The final histopathological report of the experienced uropathologist concluded that the cells that appeared viable on H&E staining were in fact non-viable and had died by thermal fixation. The most significant evidence was the negative staining with cytokeratin 8 (Cam 5.2) and AMACR antibodies, which were both positive in the residual carcinoma outside the targeted region near neurovascular bundle. To our surprise, p16 and androgen receptor stainings were weakly positive in the thermally-fixed cells but more evident in the residual carcinoma outside the treated region. Ki-67 staining showed the highest number of positively stained cells within untreated residual carcinoma, with a small number of Ki-67-positive cells also found in the thermally-fixed region, while benign tissue and CNZ were virtually negative.

Discussion

Here, we presented a case from a treat-and-resect clinical trial where the study patient presented with apparently viable cells in initial H&E-stained histology of their RP specimen after TULSA. However, analysis of MRI-thermometry, 3-week, post-TULSA NPV and immunohistochemistry concluded that in fact these cells were severely damaged and non-viable, having undergone thermal fixation. In particular, loss of cytokeratin 8 staining was indicative of severe cellular damage in both thermally-fixed and thermally-necrosed regions, and a lack of von Willebrand Factor enhancement

suggested that fixation involves cellular damage without vascular effects. While we had a small number of patients (due to the lack of patient benefit in a treat-and-resect study), our detailed description of staining outcomes in whole-mount tissues acquired three weeks after treatment with a novel ablation device provides valuable confirmation and extension of the limited available literature on thermal fixation. These observations offer important guidance for pathologists reviewing an increasing number of post-ablation histological specimens.

Table 1 summarizes our comprehensive literature search comprising all original articles discussing at least one case of thermally-fixed tissue after thermal ablation. In these studies, initial H&E-stained histopathological evaluation of ablation efficacy consistently revealed a region of tissue that appeared morphologically viable within a larger ablated region, suggesting untreated or surviving viable tissue. Several methods have been exploited to confirm that these regions represent thermally-fixed cells with severely damaged non-viable tissue, including supravital stains (TTC and NADH), IHC (in prostate; panCK, CK8, vWF, Ki-67), electron microscopy and fluorescence microscopy (Table 1). However, some of these methods are not routinely available or not feasible in clinical practice, such as electron microscopy. Furthermore, supravital stainings can only be performed on fresh tissue specimens, while fluorescence microscopy has not been validated in human tissue specimens.

In addition to our current study, there are only five human *in vivo* studies reporting thermally-fixed cells after thermal ablation: two in the prostate (six cases after HIFU and four cases after focal laser ablation), two in the liver (four cases after radiofrequency ablation and one case after HIFU) and one in the breast (11 cases after HIFU). There are no previous reports on thermal fixation for *in vivo* human

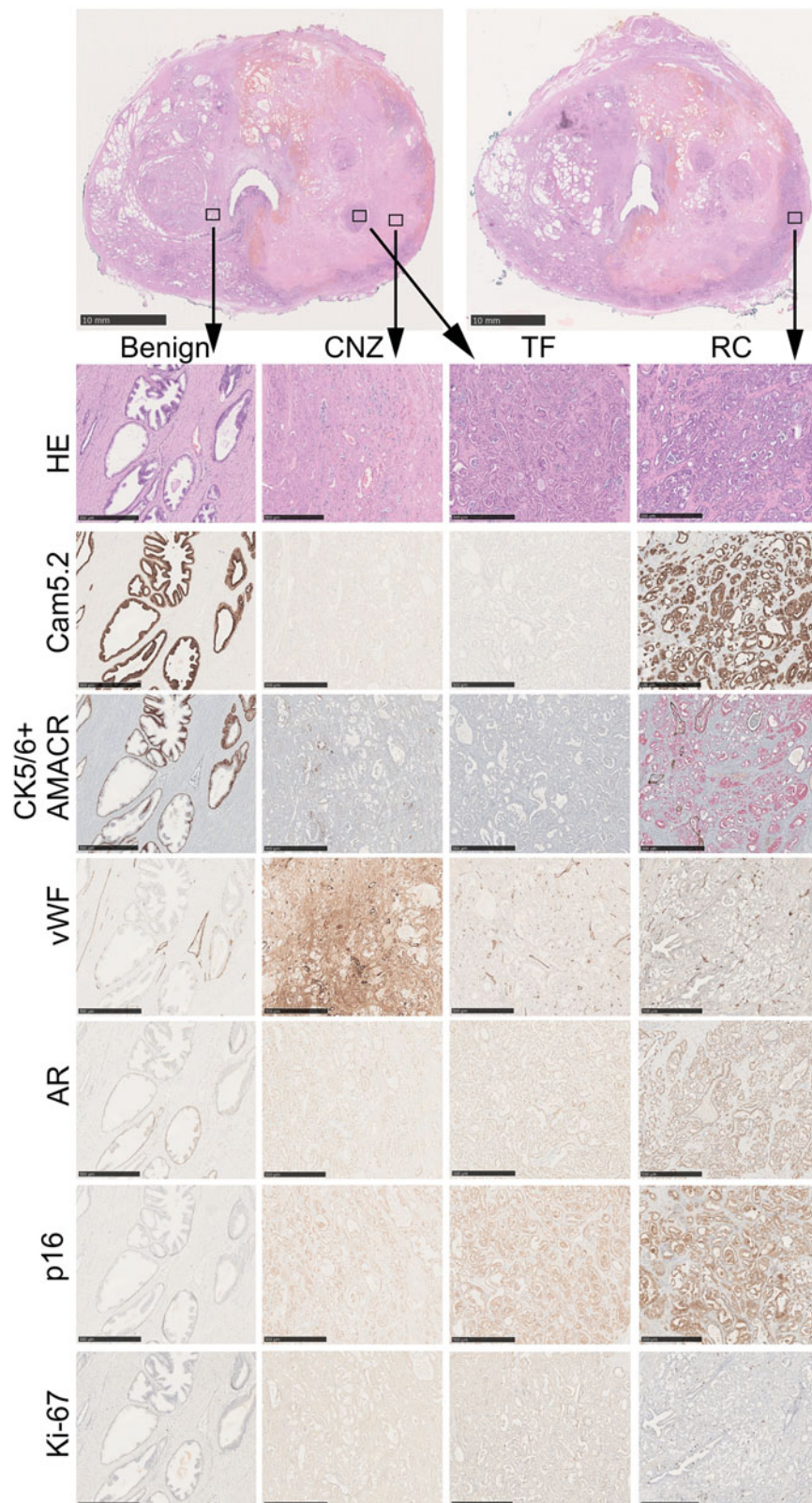


Figure 4. Immunohistochemical staining patterns of different prostatic regions after thermal injury. Two parallel HE-stained macro-sections from mid-prostate are shown from the same patient. High magnification images from benign-untreated region, coagulative necrosis zone (CNZ), thermally-fixed region (TF) and residual carcinoma (RC) with different stainings are shown below, and the defined regions are indicated with squares in the low magnification macro images. Note that there is a loss of cytokeratin 8 (Cam5.2) and AMACR staining in both CNZ and TF regions. A strong extracellular staining for vWF is seen in CNZ, while the staining is restricted to vessels in other regions. AR and p16 are weakly positive in CNZ and TF regions but virtually more abundant in RC region. Scale bar 10 mm for macro-sections, 0.5 mm for high magnification images.

Table 1. Previous literature of thermal fixation.

Authors	Therapy device	Material	Methods					Validation of thermal fixation
			SS	HP	IHC	Others		
Van Leenders et al. [16]	HIFU	9 human prostate whole glands <i>in vivo</i>		H&E; uranyl acetate; lead citrate	CK8; anti-PSA; panCK; Ki67	Electron microscopy	Thermal fixation indicated by H&E in 6 prostates; non-viability confirmed by CK8 negativity and electron microscopy	
Bhowmick et al. [29]	Heating with copper block	10 human prostate tissue samples <i>in vitro</i>		H&E		Fluorescence microscope (EthD-2 and Hoechst 33342 dyes)	Thermal fixation indicated by H&E; non-viability confirmed by fluorescence microscopy	
Boyes et al. [17]	Transurethral ultrasound	7 canine prostate whole glands <i>in vivo</i>	TTC	H&E		CE-MRI	Non-viability confirmed by TTC unstaining; thermally fixated in H&E-staining	
Lindner et al. [36]	FLA	4 human prostate whole glands <i>in vivo</i>		H&E	CK8 (CAM 5.2)	CE-MRI	Thermal fixation indicated by H&E; non-viability confirmed by CK8 negativity and CE-MRI	
Stafford et al. [31]	LITT	7 canine prostate whole glands <i>in vivo</i>		H&E	vWF	CE-MRI	Thermal fixation in every prostate in H&E; non-viability confirmed by vWF	
Germer et al. [28]	LITT	55 rabbit liver whole glands <i>in vivo</i>		H&E; silver nitrate; azan		CE-MRI	Non-viability indicated by morphology with H&E; non-viability confirmed by CE-MRI	
Coad et al. [32]	RFA	4 human liver whole glands <i>in vivo</i>		H&E		CE-MRI; CE-CT	Thermal fixation in every liver in H&E; non-viability confirmed by CE-MRI or CE-CT	
Leslie et al. [39]	HIFU	6 human liver whole glands <i>in vivo</i>	TTC	H&E	Factor VIII	CE-MRI	Thermal fixation in 1 indicated by lack of post-mortem autolysis in morphology; non-viability confirmed by Factor VIII and CE-MRI	
Courivaud et al. [35]	HIFU	4 + 5 swine liver whole glands <i>in vivo</i> ^a		H&E		CE-MRI	Thermal fixation in 7 livers in H&E; non-viability confirmed by CE-MRI and by presence of foreign-body giant cells	
Hennings et al. [30]	CITT	8 nipples of one swine <i>in vivo</i> ; 8 rabbit VX2 carcinomas <i>in vivo</i>	TTC	H&E	Anti-PCNA	Autofluorescence microscopy	Thermal fixation indicated by H&E; non-viability confirmed by TTC and autofluorescence microscopy	
He et al. [34]	MW thermal therapy	5 + 7+8 porcine kidneys <i>in vitro</i> or <i>in vivo</i> ^b		H&E			Thermal fixation in every kidney; non-viability indicated by morphology with H&E	
Wu et al. [37]	HIFU	23 human breast whole organ <i>in vivo</i>	NADH	Uranyl acetate; lead citrate; H&E	biotin-streptavidin-peroxidase; CA15-3; VEGF	Electron microscopy	Thermal fixation in 11 breast tumors indicated by H&E; non-viability confirmed by NADH and electron microscopy	

Therapy device: HIFU = high-intensity focused ultrasound, LITT = laser interstitial thermal therapy, FLA = focal laser ablation, RFA = radiofrequency ablation, CITT = conductive interstitial thermal therapy, MW = microwave; Supravital staining (SS); TTC = triphenyl tetrazolium chloride, NADH = nicotinamide adenine dinucleotide; Histopathology (HP); H&E = hematoxylin-eosin; ICH = immunohistochemistry; CK = cytokeratin, PSA = prostate-specific antigen, vWF = von Willebrand factor, PCNA = proliferating nuclear antigen, CE-MRI = contrast-enhanced magnetic resonance imaging.

^aFour ablated and euthanized after immediate MR; five *in vivo* study, euthanized after 1-wk MRI.

^bFour animals, five kidneys *in vitro*; six animals, seven kidneys *in vivo* 2-h perfusion; four animals, eight kidneys *in vivo* 7-d perfusion.

prostate using transurethral ultrasound therapy, which has distinct patterns of thermal dose deposition and histological damage due to the use of continuous heating with an unfocused ultrasound beam (as opposed to a series of brief small volume exposures in HIFU).

Specific to prostate tissue, two other *in vivo* studies and one *in vitro* study have reported thermally-fixed cells in human prostates after thermal ablation, and one additional *in vivo* study reported findings in canine prostates. In both *in vivo* human studies, cytokeratin 8 staining was utilized for detecting non-viable dead tissue [16,36]. Van Leenders et al. [16] demonstrated an apparent concordance between cytokeratin 8-negative prostate tissue inside ablated area and ultrastructural electron microscopy changes consistent with necrosis. Based on our results and the conclusions of these studies, cytokeratin 8, as detected by Cam5.2 antibody, appears more sensitive for detection of necrosis than H&E staining, identifying cells that are non-viable despite retaining normal morphologic features on H&E. Following transurethral ultrasound ablation in canine prostates, Boyes et al. [17] observed a TFZ located in the central area of the CNZ where the highest temperature is likely to occur, and more prominent when large target boundaries result in faster temperature rise and higher temperatures enabling formation of thermal fixation. In our study, a distinct TFZ was distinguishable in only one patient, but was similarly located within the CNZ in the region with the highest maximum temperature. This patient also had the most rapid temperature rise among the six study patients, possibly related to a large intended treatment volume as suggested by Boyes et al. [17].

Besides traditional therapies (RP, RT, brachytherapy), FTs have emerged as a potential therapeutic option in localized PCa with the main purpose of selective tumor ablation with equivalent oncological control, reduced toxicity and improved functional outcomes. Remaining challenges for organ-sparing ablation strategies include determining how to ensure oncological safety and how to optimize follow-up of oncological outcomes in both in-field and out-of-field regions. Apart from imaging and PSA, consensus guidelines recommend using follow-up biopsy specimens from the ablated region to assess treatment outcome [6]. However, histopathological assessment of biopsy specimens after thermal ablation may be confounded by thermally-fixed cells that appear to be viable on H&E staining. The prevalence of thermally-fixed tissue in prostate biopsy specimens after thermal ablation is unknown. Furthermore, it is not known how long thermally-fixed cells can retain apparently viable morphology after thermal ablation. In liver tissue, the appearance of thermal fixation can remain up to at least 14 months post-ablation [32]. If this finding applies also in the prostate, one could speculate on the possibility of detecting thermally-fixed non-viable cells in post-ablation biopsy specimens. This would have important clinical implications, since guidelines suggest the use of serial follow-up biopsies from the ablated area as a defining component of surveillance after prostate focal therapy [6,53].

Although heat exposure is increasingly being utilized in PCa management, both the phenomenon of thermal fixation

and its incidence are poorly known in clinical practice. Currently, there is no standard method to determine the viability of heat-fixed cells, which may lead to incorrect diagnosis of treatment failure when pathologists assess biopsy specimens from thermally-ablated regions. Several supplemental histopathological examinations have suggested that thermally-fixed cells represent non-viable dead tissue, including supravital stains, autofluorescence, electron microscopy and IHC from apparently viable regions suspected to present thermal fixation. In particular, the results of our study and others in human prostate cancer have demonstrated that a loss of cytokeratin 8 staining in glandular epithelium after thermal ablation indicates severe cellular damage and correlates with necrosis in ultrastructural examinations (Table 1). However, it is important to note that while Cam5.2 has primary reactivity with cytokeratin 8, it is also reactive with cytokeratin 7, yet there is no published literature about the utility of cytokeratin 8 antibodies other than Cam5.2 in detecting thermally-fixed cells. Since the negative staining is presumably due to loss of antigenicity for Cam5.2 antibody rather than true lack of cytokeratin 8 itself, this pitfall needs to be considered in clinical diagnosis of post-ablation histological specimens. A loss of AMACR staining in thermally-fixed cells may also be helpful, but cannot be considered ground truth as approximately 10% of adenocarcinomas appear AMACR negative. While these stains offer practical tools for assessing cells that appear viable within regions of intense thermal damage, there is still a need for further development, standardization and utilization of histological markers of thermal fixation.

Conclusion

Thermally-fixed cells can appear viable due to sustained morphological detail on H&E staining after thermal ablation. Interpretation of prostate specimens after thermal ablation may suggest treatment failure, if this effect is not recognized and ancillary immunohistochemistry performed. Based on the previous literature and the current study, cytokeratin 8 (Cam5.2) and AMACR staining appear practical and reliable tools for distinguishing thermally-fixed non-viable cells from viable cells.

Disclosure statement

No potential conflict of interest was reported by the authors.

ORCID

Mikael Anttinen  <http://orcid.org/0000-0002-9351-7177>
 Visa Suomi  <http://orcid.org/0000-0002-1300-3425>

References

- [1] Bill-Axelsson A, Holmberg L, Garmo H, et al. Radical prostatectomy or watchful waiting in early prostate cancer. *New Eng J Med.* 2014;370:932–942.

- [2] Wilt TJ, Jones KM, Barry MJ, et al. Follow-up of prostatectomy versus observation for early prostate cancer. *N Engl J Med.* 2017; 377:132–142.
- [3] Hamdy FC, Donovan JL, Lane JA, et al. 10-year outcomes after monitoring, surgery, or radiotherapy for localized prostate cancer. *N Engl J Med.* 2016;375:1415–1424.
- [4] Donovan JL, Hamdy FC, Lane JA, et al. Patient-reported outcomes after monitoring, surgery, or radiotherapy for prostate cancer. *N Engl J Med.* 2016;375:1425–1437.
- [5] Sanda MG, Dunn RL, Michalski J, et al. Quality of life and satisfaction with outcome among prostate-cancer survivors. *N Engl J Med.* 2008;358:1250–1261.
- [6] van der Poel MG, Henk G, van den Bergh RCN, Briers E, et al. Focal therapy in primary localised prostate cancer: the European Association of Urology position in 2018. *Eur Urol.* 2018;74:84–91.
- [7] Valerio M, Cerantola Y, Eggner SE, et al. New and established technology in focal ablation of the prostate: a systematic review. *Eur Urol.* 2017;71:17–34.
- [8] Woodrum DA, Gorny KR, Mynderse LA. Mr-guided Prostate Interventions. *Top Magn Reson Imaging.* 2018;27:141–151.
- [9] Ahmed HU, Bosaily AE, Brown LC, et al. Diagnostic accuracy of multi-parametric MRI and TRUS biopsy in prostate cancer (PROMIS): a paired validating confirmatory study. *Lancet.* 2017; 389:815–822.
- [10] Kasivisvanathan V, Rannikko AS, Borghi M, et al. MRI-targeted or standard biopsy for prostate-cancer diagnosis. *N Engl J Med.* 2018;378:1767–1777.
- [11] Ramsay E, Mougenot C, Staruch R, et al. Evaluation of focal ablation of magnetic resonance imaging defined prostate cancer using magnetic resonance imaging controlled transurethral ultrasound therapy with prostatectomy as the reference standard. *J Urol.* 2017;197:255–261.
- [12] Chopra R, Colquhoun A, Burtnyk M, et al. MR imaging–controlled transurethral ultrasound therapy for conformal treatment of prostate tissue: Initial feasibility in humans. *Radiology.* 2012;265: 303–313.
- [13] Chin JL, Billia M, Relle J, et al. Magnetic resonance imaging-guided transurethral ultrasound ablation of prostate tissue in patients with localized prostate cancer: a prospective phase 1 clinical trial. *Eur Urol.* 2016;70:447–455.
- [14] Ross AB, Diederich CJ, Nau WH, et al. Highly directional transurethral ultrasound applicators with rotational control for MRI-guided prostatic thermal therapy. *Phys Med Biol.* 2004;49:189.
- [15] Chu KF, Dupuy DE. Thermal ablation of tumours: biological mechanisms and advances in therapy. *Nat Rev Cancer.* 2014;14: 199–208.
- [16] Van Leenders G, Beerlage HP, Ruijter ET, et al. Histopathological changes associated with high intensity focused ultrasound (HIFU) treatment for localised adenocarcinoma of the prostate. *J Clin Pathol.* 2000;53:391–394.
- [17] Boyes A, Tang K, Yaffe M, et al. Prostate tissue analysis immediately following magnetic resonance imaging guided transurethral ultrasound thermal therapy. *J Urol.* 2007;178:1080–1085.
- [18] Burtnyk M, Hill T, Cadieux-Pitre H, et al. Magnetic resonance image guided transurethral ultrasound prostate ablation: a pre-clinical safety and feasibility study with 28-day followup. *J Urol.* 2015;193:1669–1675.
- [19] Ishihara Y, Calderon A, Watanabe H, et al. A precise and fast temperature mapping using water proton chemical shift. *Magn Reson Med.* 1995;34:814–823.
- [20] Ramsay E, Mougenot C, Köhler M, et al. MR thermometry in the human prostate gland at 3.0 T for transurethral ultrasound therapy. *J Magn Reson Imaging.* 2013;38:1564–1571.
- [21] Siddiqui K, Chopra R, Vedula S, et al. MRI-guided transurethral ultrasound therapy of the prostate gland using real-time thermal mapping: initial studies. *Urology.* 2010;76:1506–1511.
- [22] Chopra R, Tang K, Burtnyk M, et al. Analysis of the spatial and temporal accuracy of heating in the prostate gland using transurethral ultrasound therapy and active MR temperature feedback. *Phys Med Biol.* 2009;54:2615.
- [23] Böni RA, Sulser T, Jochum W, et al. Laser ablation-induced changes in the prostate: findings at endorectal MR imaging with histologic correlation. *Radiology.* 1997;202:232–236.
- [24] Rouvière O, Lyonnet D, Raudrant A, et al. MRI appearance of prostate following transrectal HIFU ablation of localized cancer. *Eur Urol.* 2001;40:265–274.
- [25] Bomers JGR, Cornel EB, Futterer JJ, et al. MRI-guided focal laser ablation for prostate cancer followed by radical prostatectomy: correlation of treatment effects with imaging. *World J Urol.* 2017; 35:703–711.
- [26] Rosset R, Bratan F, Crouzet S, et al. Can pre-and postoperative magnetic resonance imaging predict recurrence-free survival after whole-gland high-intensity focused ablation for prostate cancer? *Eur Radiol.* 2017;27:1768–1775.
- [27] Biermann K, Montironi R, Lopez-Beltran A, et al. Histopathological findings after treatment of prostate cancer using high-intensity focused ultrasound (HIFU). *Prostate.* 2010;70:1196–1200.
- [28] Germer C, Isbert CM, Albrecht D, et al. Laser-induced thermotherapy for the treatment of liver metastasis. *Surg Endoscopy.* 1998; 12:1317–1325.
- [29] Bhowmick S, Coad JE, Swanlund DJ, et al. *In vitro* thermal therapy of AT-1 Dunning prostate tumours. *Int J Hyperthermia.* 2004;20: 73–92.
- [30] Hennings L, Kaufmann Y, Griffin R, et al. Dead or alive? Autofluorescence distinguishes heat-fixed from viable cells. *Int J Hyperthermia.* 2009;25:355–363.
- [31] Stafford RJ, Shetty A, Elliott AM, et al. Magnetic resonance guided, focal laser induced interstitial thermal therapy in a canine prostate model. *J Urol.* 2010;184:1514–1520.
- [32] Coad JE, Kosari K, Humar A, et al. Radiofrequency ablation causes ‘thermal fixation’ of hepatocellular carcinoma: a post-liver transplant histopathologic study. *Clin Transplant.* 2003;17:377–384.
- [33] Coad JE. Thermal fixation: a central outcome of hyperthermic therapies. *Proceedings of Thermal Treatment of Tissue: Energy Delivery and Assessment III.* International Society for Optics and Photonics. 2005. Vol. 5698. p. 15–22.
- [34] He X, McGee S, Coad JE, et al. Investigation of the thermal and tissue injury behaviour in microwave thermal therapy using a porcine kidney model. *Int J Hyperthermia.* 2004;20:567–593.
- [35] Courivaud F, Kazaryan AM, Lund A, et al. Thermal fixation of swine liver tissue after magnetic resonance-guided high-intensity focused ultrasound ablation. *Ultrasound Med Biol.* 2014;40: 1564–1577.
- [36] Lindner U, Lawrentschuk N, Weersink RA, et al. Focal laser ablation for prostate cancer followed by radical prostatectomy: validation of focal therapy and imaging accuracy. *Eur Urol.* 2010;57: 1111–1114.
- [37] Wu F, Wang Z, Cao Y, et al. Heat fixation of cancer cells ablated with high-intensity-focused ultrasound in patients with breast cancer. *Am J Surg.* 2006;192:179–184.
- [38] Künzli B, Abitabile MP, Maurer CA. Radiofrequency ablation of liver tumors: actual limitations and potential solutions in the future. *WJH.* 2011;3:8–14.
- [39] Leslie TA, Kennedy JE, Illing RO, et al. High-intensity focused ultrasound ablation of liver tumours: can radiological assessment predict the histological response? *BJR.* 2008;81:564–571.
- [40] van Vulpen M, Raaymakers BW, de Leeuw AA, et al. Prostate perfusion in patients with locally advanced prostate carcinoma treated with different hyperthermia techniques. *J Urol.* 2002;168: 1597–1602.
- [41] Sapareto SA, Dewey WC. Thermal dose determination in cancer therapy. *Int J Radiat Oncol• Biol• Phys.* 1984;10:787–800.
- [42] Dewhurst MW, Viglianti BL, Lora-Michiels M, et al. Basic principles of thermal dosimetry and thermal thresholds for tissue damage from hyperthermia. *Int J Hyperthermia.* 2003;19:267–294.

- [43] Damianou C, Hynynen K. The effect of various physical parameters on the size and shape of necrosed tissue volume during ultrasound surgery. *J Acoust Soc Am.* 1994;95:1641–1649.
- [44] Fan X, Hynynen K. Ultrasound surgery using multiple sonications—treatment time considerations. *Ultrasound Med Biol.* 1996; 22:471–482.
- [45] Yarmolenko PS, Moon EJ, Landon C, et al. Thresholds for thermal damage to normal tissues: an update. *Int J Hyperthermia.* 2011; 27:320–343.
- [46] Li GC, Mivechi NF, Weitzel G. Heat shock proteins, thermotolerance, and their relevance to clinical hyperthermia. *Int J Hyperthermia.* 1995;11:459–488.
- [47] Borrelli MJ, Thompson LL, Cain CA, et al. Time-temperature analysis of cell killing of BHK cells heated at temperatures in the range of 43.5 C to 57.0 C. *Int J Rad Oncol* Biol* Phys.* 1990;19: 389–399.
- [48] Field SB, Morris CC. The relationship between heating time and temperature: its relevance to clinical hyperthermia. *Radiother Oncol.* 1983;1:179–186.
- [49] Majno G, Joris I. Apoptosis, oncosis, and necrosis. An overview of cell death. *Am J Pathol.* 1995;146:3–15.
- [50] Vykhodtseva N, Mcdannold N, Martin H, et al. Apoptosis in ultrasound-produced threshold lesions in the rabbit brain. *Ultrasound Med Biol.* 2001;27:111–117.
- [51] Wall MS, Deng X, Torzilli PA, et al. Thermal modification of collagen. *J Shoulder Elbow Surg.* 1999;8: 339–344.
- [52] Wright NT, Humphrey JD. Denaturation of collagen via heating: an irreversible rate process. *Annu Rev Biomed Eng.* 2002;4: 109–128.
- [53] Tay KJ, Amin MB, Ghai S, et al. Surveillance after prostate focal therapy. *World J Urol.* 2019;37:397–407.